Nowcasting of Motion and Growth of Precipitation with Radar over a Complex Orography

Article *in* Journal of Applied Meteorology · June 1995

DOI: 10.1175/1520-0450(1995)034<1286:NOMAGO>2.0.CO;2

3 authors, including:

Willi Schmid
meteoradar gmbh
54 PUBLICATIONS **1,360** CITATIONS

SEE PROFILE

Statistical Properties of Rain Cells in the Padana Valley

CARLO CAPSONI, MICHELE D'AMICO, AND PAOLO LOCATELLI

Politecnico di Milano, DEI, Milano, Italy

(Manuscript received 4 March 2008, in final form 16 May 2008)

ABSTRACT

A large collection of radar reflectivity maps gathered from 1988 to 1992 at the Spino d'Adda experimental station, located in the Padana Valley, has been exploited to investigate the statistical properties of rain structures and their descriptors. The results of this analysis can be of interest for meteorological, hydrological, and telecommunication applications. The authors found that the isosuperficial diameter follows an exponential distribution; when the threshold of rain intensity is increased, disappearance is dominant over fragmentation; moreover, the number of "mother cells" that generate N "daughter cells" decreases exponentially with N. To give a complete but concise characterization of the geometrical, physical, and morphological properties of rain cells, a set of analytical descriptors has been introduced and statistically defined through their probability density functions and the centrality, dispersion, and excursion parameters. As a final point, comparative statistical analyses have been performed at different thresholds for every couple of descriptors introduced, which allowed the authors to highlight correlations between them.

1. Introduction

Meteorological radars can monitor wide geographic areas with high spatial and temporal resolution, providing detailed information on the spatial structure of precipitation; this information is of concern in radio wave propagation (for the design of modern radio communication systems), in hydrology, climatology, and weather now- and forecasting. However, the raw data gathered by the radar system (radar reflectivity) need a great amount of complex processing to provide the desired information with the spatial/temporal characteristics that are needed to extract suitable descriptors (Pawlina 1987, 1990). In hydrology, reliable information on the physical and morphological properties of rain structures, as well as their time and space evolution, is useful to initialize runoff models and for applications such as the control of water level in lakes and the flood forecasting of river catchments (Borga et al. 2000; Mecklenburg et al. 2000). In telecommunication applications, the knowledge of the statistical characteristics of rain structures is needed as basic input for propagation models at centimeter and millimeter wavelengths (Oguchi 1983). Information about structures inside the rain fields (such as size, shape, and orientation of rain cells) permits one to accurately model and simulate the spatial inhomogeneity of rain fields in order to select the best fade mitigation technique for both ground and space communication systems (Goldhirsh 1982, 1983; Khamis et al. 2005; Pawlina 1998).

The ability to describe rain fields over a wide range of spatial scales has become of great importance for the effective exploitation of advanced techniques in satellite-based broadcasting and multimedia telecommunication services such as onboard resource sharing, space or route diversity, and adaptive antenna footprinting (Paraboni et al. 2002).

The shape of rain cells represents a crucial input for stochastic point-process models that describe intense precipitation events (Capsoni et al. 1987a; Feral et al. 2000; Montopoli et al. 2006). Furthermore, the comparison between shapes of real and simulated rain cells can be considered an additional way to assess the performances of high-resolution meteorological models.

In this work, a set of analytical descriptors has been introduced to provide a complete but very concise description of the geometrical, physical, and morphological characteristics of the rain structures. They are area, perimeter, peak and average value of rain rate, cell dynamic and diffusion, cell ellipticity, and solidity. In

Corresponding author address: Prof. Michele D'Amico, Politecnico di Milano, DEI, Piazza L. da Vinci 32, Milano 20133, Italy.
E-mail: damico@elet.polimi.it

DOI: 10.1175/2008JTECHA1130.1

section 2 we describe the radar characteristics and the procedure adopted to extract rain structures from the radar maps. In section 3 we discuss the characteristics of the (two) generated databases and the analyses performed to assess their correctness and statistical completeness. Section 4 introduces the set of descriptors listed above, giving their definition, the rationale for their choice, and their possible applications in hydrological and propagation models. Section 5 is devoted to structure analyses, including the cumulative distributions of rain cell sizes for the different rain-rate categories and the study of fragmentation and disappearance of cells as functions of the threshold. The cell descriptors are investigated in section 6, where we present their complete statistical description and their joint statistics for different rain-rate thresholds.

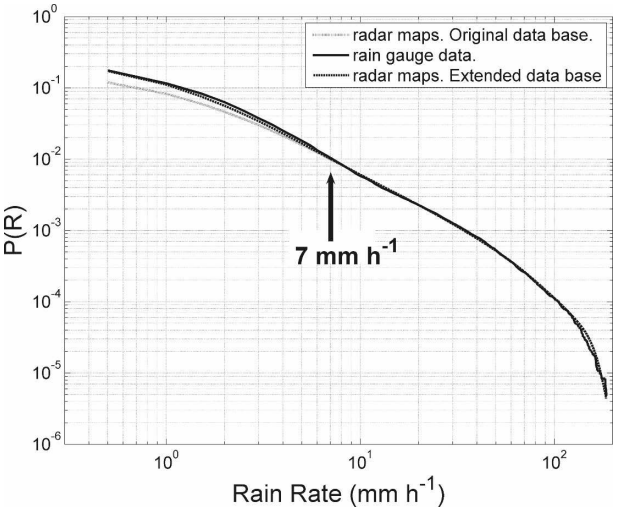

FIG. 1. Cumulative point rainfall rate distribution calculated from radar maps compared with that obtained from the rain gauge; the fit is forced at 20 mm h^{-1}.

2. The radar database

The database used in this study was collected by the S-band Doppler single polarization meteorological radar installed in the experimental station of Spino d'Adda, 30 km southeast of Milan, during the period June 1988–February 1992. Some technical details of the equipment are the frequency of operation (2.8 GHz), peak power (475 kW), pulse duration (0.5 μs), pulse repetition frequency (PRF; 500/1000 Hz), antenna beamwidth (2° at −3 dB), and minimum detectable signal (MDS; −104 dBm). This equipment covers an area of about 150 km in radius; however, to obtain images almost free from ground clutter and with high spatial resolution, only the central portion of this region is considered in this work: the presence of the Alps (north) and of the Apennines (south) limits the maximum clutter-free region to a circle 40 km in radius.

Reflectivity maps were generated by combining three plan position indicator (PPI) scans taken at 3°, 5°, and 7° of elevation into a pseudo-CAPPI (constant altitude PPI) at 1.5 km of height. For distances smaller than 10 km we used data from the 7° elevation; in this case the actual height of the center of the radar cell is lower than 1.5 km; however, the impact of this approximation is negligible, if the vertical structure of precipitation is reasonably uniform. Radar reflectivity Z (mm^6 m^{-3}) was converted into rain-rate R (mm h^{-1}) using the Marshall–Palmer relation $Z = 200R^{1.6}$, which was proven to be very suitable on a statistical basis in the meteorological contest of the Padana Valley (Pawlina 1984). The minimum threshold in rain rate was set at 0.5 mm h^{-1}. Maps, initially collected in polar form, were converted into a Cartesian grid having a resolution of 500 m × 500 m. Each pixel of these maps represents the value of average rain intensity measured in the space volume surrounding the grid element. Isolated pixels contaminated by clutter were replaced by the value of rain rate obtained by linear interpolation of the adjacent ones. During the observation period 54 rain events were collected, corresponding to 15 098 radar maps containing rain. The time interval between two successive maps is 77 s, which leads to about 323 h of observation.

3. Database validation and conditioning

As a first step toward validation of the radar database, the cumulative distribution function (CDF) of rain intensity was calculated and compared with that obtained from data collected—in the same period—by a tipping-bucket rain gauge collocated with the radar (Pawlina 1999). The two curves, showing the probability that the value of rain rate in abscissa is exceeded, are plotted in Fig. 1; the radar curve (dotted line) is normalized to the rain gauge data (solid line) forcing fit at 20 mm h^{-1}. The radar and the rain gauge distributions show an excellent agreement for rain-rate values higher than 7 mm h^{-1}; for lower intensities the radar tends to slightly underestimate rain intensity (for a given probability) with respect to the rain gauge; this can be due to the fact that some very light, stratiform events that occurred during the observation period were not recorded by the radar. The reason for lack of data is that at the Spino d'Adda research facility, the radar was not operated continuously (24 h, 7 days a week), but was activated only in coincidence of significant precipitation events (in terms of intensity and/or duration); very light and very short events were purposely missed.

Therefore, to avoid introducing possible biases in the statistics, the original database has been modified by adding "synthetic" events obtained by duplicating existing ones, following a procedure outlined in Fukuchi et al. (2000). We have chosen which rain events to duplicate, and how many times, by adopting the following guidelines: rain events must be stratiform, with a prevailing rain intensity lower than 7 mm h^{-1}; the whole rain event must be duplicated, and not isolated radar pictures; and it is preferable to repeat a large number of different rain events a few times, rather than repeating a few of them many times.

At the end of the duplication procedure we obtained an extended radar database constituted by 81 rain events corresponding to 21 958 radar pictures, for a total of about 465 h of observation; the radar-derived CDF (dashed line in Fig. 1) now shows an excellent agreement with that obtained from the rain gauge over the whole range of rain-rate values.

The extended database is climatologically representative because it is formed by rain events collected in different months of the year and in different years, thus guaranteeing the presence both of stratiform and convective events (Matricciani and Pawlina 2000). Moreover, in section 5 we show how this extension procedure has only a minor impact on the statistical properties of the cell descriptors, leading to results that are comparable with those present in the literature.

The rain cells

The term "rain cell" refers to a set of connected pixels, extracted from each radar map, whose rain-rate value exceeds a given threshold (Goldhirsh and Musiani 1992; Sauvageout et al. 1999). The thresholds chosen in this work are 0.5, 1, 3, 5, 10, 20, and 30 mm h^{-1}. A rain cell is considered uncorrupted and then stored in the database; it is not cut by the radar observation window and it is larger than 5 km^2. The first constraint has to be introduced to ensure that the descriptors of rain cells stored are correct, while the second constraint leads to ignored cells that are too small to be significant. To satisfy the requirements requested by the successive analyses two different types of databases have been generated: the "complete" database includes all the rain cells, and the "partial" database includes only those cells that admit a mother cell at the (immediately) lower threshold. For example, the complete database at 3 mm h^{-1} is composed by the totality of rain cells identified by that threshold and that are uncorrupted; the corresponding partial database is a subset (of the complete one) and includes only rain cells coming from uncorrupted mother cells (i.e., rain cells at 1 mm h^{-1}). Table 1 shows the cardinality of the databases, classifying the rain cells by their threshold.

TABLE 1. Number of rain cells collected in the databases classified for type and threshold.

	Databases					
	Partial database					
Threshold (mm h^{-1})	Minimum threshold (mm h^{-1})					Complete database
	0.5	1	3	5	10	
0.5	50 117					50 117
1	22 974	46 794				46 794
3	4038	7290	26 032			26 032
5	1709	2870	10 003	17 206		17 206
10	627	1074	2769	4917	9118	9118
20	302	486	1087	1721	3120	4357
30	165	295	663	1011	1773	3016
Total	79 932	58 809	40 554	24 855	14 011	156 640

As mentioned above, the databases include only rain cells fully contained in the observation area, a 40-km-radius circle. Since the probability of intersecting the window border is higher for large cells with respect to small ones, a statistical bias can be introduced. This bias has been removed following the procedure outlined in Capsoni et al. (1987a): each rain structure is defined for an equivalent radius $\xi(A) = (A/\pi)^{1/2}$, where A is the area of the cell; the cell is entirely contained in the observation window if its center falls within a circle (centered with the radar) whose radius is $(40 - \xi)$ km. Structures with different areas are therefore characterized by different effective observation windows. To remove this bias, the number density of each class of radar cells has been multiplied by the correction factor $p(\xi) = [40/(40 - \xi)]^2$.

4. Rain cell descriptors

A set of descriptors is associated with every rain cell in the databases that is useful both to locate it inside the radar maps and to characterize its statistical features. Information such as the rain map from which the structure is extracted, the threshold applied, and the centroid coordinates are useful for a first-level identification of the structures; moreover, a set of descriptors that are linked to geometrical, physical, and morphological characteristics of rain structures are associated with each rain cell in the database. Various descriptors can be unambiguously defined for a given rain cell; in this work these have been considered: area A, perimeter P, peak and average value of rain rate (R_P and R_M, respectively), cell dynamic D_Y, ellipticity E_L, diffusion D_I, and solidity S_O.

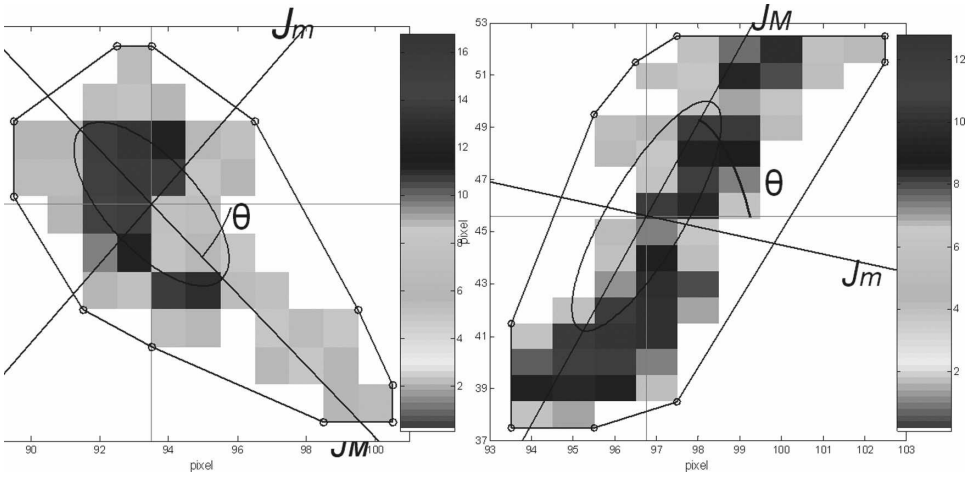

FIG. 2. Direction of the principal moments of inertia (J_M and J_m), inertial ellipse, orientation angle (θ), and circumscribed convex polygon.

Since the size of the square pixels of the radar maps is 0.5 km $\times$ 0.5 km, the area A (km^2) of the rain cell is equal to the number of pixels divided by four; the perimeter P (km) is equal to the number of contour rainy pixels divided by two. In accordance with the integrity constraints (section 3), the rain cells collected in the databases have an area $A \geq 5$ km^2 and perimeter $P \geq 9$ km. Peak and average rain rate (mm h^{-1}) must assume values larger than the threshold for which the cell is defined.

Cell dynamic D_Y is defined as the ratio between average and peak rain rate (i.e., $D_Y = R_M/R_P$); it assumes values close to one for flat structures and very small values for structures with high dynamics.

The ellipticity factor E_L, the most common shape descriptor, is defined as the ratio between J_m and J_M, the minimum and maximum value of the rain cell principal moment of inertia (Feral et al. 2000; Capsoni and D'Amico 2004), respectively. The ellipticity is a normalized parameter that assumes values close to zero for structures with a highly elongated form.

The diffusion descriptor D_I is defined as

$$D_I = \frac{J_M - J_m}{A^2} \ (\text{mm h}^{-1}\ \text{km}^{-2}) \qquad (1)$$

and it is related to the inertial principal moments. It gives information on how the water masses are distributed within the rain structure by taking into account both their relative position and amount. This descriptor assumes high values for structures with very elongated form and high dynamic.

The morphological features of rain cells are also described through solidity S_O, defined as the ratio between the area A of the structure and the area of the smallest circumscribed convex polygon (see Fig. 2). It is a normalized parameter that is sensitive to the spatial complexity of a rain cell.

This set of descriptors provides a very concise but complete characterization of rain cells. Other morphological parameters introduced in Capsoni and D'Amico (2004) have not been considered here because they do not supply any additional information about the cells because they are related to ellipticity and solidity. An illustration of the inertial principal moment directions, the circumscribed convex polygon, and the inertial ellipse and its orientation for rain cells of different shape is presented in Fig. 2. The orientation angle of the cells (defined as the angle formed between the major axis and the east direction) has been found to be almost uniformly distributed, and independent of the thresholds and the other rain descriptors (Konrad 1978; Feral et al. 2000; Capsoni and D'Amico 2004; Montopoli et al. 2006), with only a slight preference for the directions between 10° and 40° with respect to north.

The physical and geometrical descriptors can be exploited to classify the rain event as stratiform or convective (or a combination); to calculate the cumulated rain associated with a cell; and to identify the stages of birth, life, and death of cells. This information represents basic input for the algorithms of now- and forecasting (Li et al. 1995; Franchi et al. 1996; Dell'Acqua et al. 1997), for the assessment of the attenuation in the microwave propagation models (Capsoni et al. 1987b; Davarian 1994; Pawlina 1999), and for the parameterization of the water and energy cycles in the atmospheric circulation (Georgakakos and Krajewski 1996; Cheng and Arakawa 1997). The morphological descriptors can be exploited to analyze the temporal evolution

of the rain cell shape in order to track its continuous transformation that can lead to cell splitting and merging. This information is fundamental for the development of morphing algorithms for the reconstruction of the intermediate steps (missing scenes) in the morphological change of a cell, when only its starting and final shapes are known (Dell'Acqua and Gamba 1998; Belongie et al. 2002). These techniques can be useful for hydrological applications, where rain fields must be known with spatial and temporal resolutions higher than those usually provided by rain gauge networks and ground radars.

5. Structures analyses

Exploiting the huge quantity of information stored in the databases, statistical analyses have been performed on rain cells at different rain-rate thresholds to better characterize the collection of structures and to validate it by comparing the results with those available in the open literature.

a. Statistics of the rain cell sizes

The rain cell size distribution is a very informative parameter for the description of rain fields. Most of the authors have considered the isosuperficial diameter, defined as the diameter of an equivalent circular cell with area equal to that of the actual one; several studies have been published in the past; they were carried out mainly using ground radar data collected in different part of the world. Restricting the investigation to the studies performed in the temperate zone (between 32° and 53°N), the rain cell diameter distribution (RCDD) function can be assumed to follow the exponential form

$$N(D, s) = N_0(s)e^{-\lambda(s)D}, \tag{2}$$

where D is the isosuperficial diameter (measured in km), s is the threshold (in mm h^{-1}), and N_0 and λ are the two parameters of the distribution (i.e., the intercept and the slope), respectively. Both N_0 and λ can depend—in principle—on the threshold; the N_0 parameter was found to depend on the radar location; the λ parameter depends mainly on the range of rain cell sizes used for its computation, while it is only weakly dependent on the threshold and on the location. Studies performed in different locations and considering isosuperficial diameters ranging between 2 and 15 km have found values of λ between 0.22 and 0.50 km^{-1} (Konrad 1978; Goldhirsh and Musiani 1986, 1992; Pawlina 1999; Sauvageout et al. 1999; Khamis et al. 2005).

We have first evaluated the RCDD for our dataset. Although the database admits rain cells with areas between 5 and 888.5 km^2, corresponding to $2.52 \leq D \leq 33.6$ km, we preferred to restrict the analysis to values of isosuperficial diameter lower than 20 km (for data cardinality reasons) and the curve fitting to diameters smaller than 15 km, to be consistent with the results presented in literature. Such distribution, presented in Fig. 3, shows a decreasing, almost linear behavior on the semilogarithmic scale that can be optimally approximated by the exponential form in Eq. (2), with $\lambda = 0.319\ km^{-1}$. The correlation coefficient is 0.996 and the standard error equal to 4.8%; both the exponential form of the distribution and the value of the λ parameter agree well with the literature.

Figure 4 shows the average, median, and 90th percentile isosuperficial diameter as a function of rain-rate threshold, varied between 0.5 and 100 mm h^{-1}. Both the average and the median values are only weakly dependent on the threshold, consistently with Goldhirsh and Musiani (1986); this is due to the presence of a large number of isolated rain cells even at the smaller rain-rate thresholds. On the contrary, the 90th percentile curve shows a stronger dependence on the threshold, decreasing as the rain rate increases; this is due to the fact that the number of very large structures decreases significantly when the threshold increases (Drufuca and Pawlina 1976). The average values of the average, median, and 90th percentile (calculated over the entire threshold range) are equal to 4.57, 3.77, and 7.58 km, respectively.

b. Mothers and daughters

The following analyses have been carried out to investigate the parental relationships among rain cells (i.e., to identify and statically characterize mothers and daughters); please note that in our meaning a daughter cell is an intensive substructure immersed within a larger structure that exists at the (immediately) lower threshold. Therefore, with this definition the daughter cells are not related to the evolution in time of their mother cells. For these analyses we have exploited the partial databases (that include only cells that admit a mother). Figure 5 shows the number of rain cells as a function of the threshold for the complete and the partial databases; the thick line corresponds to the complete database, while the five thin lines correspond to partial databases constructed adopting five different initial thresholds (0.5, 1, 3, 5, and 10 mm h^{-1}). Each curve shows a linear decreasing behavior on a logarithmic scale with a slope independent from the particular partial database.

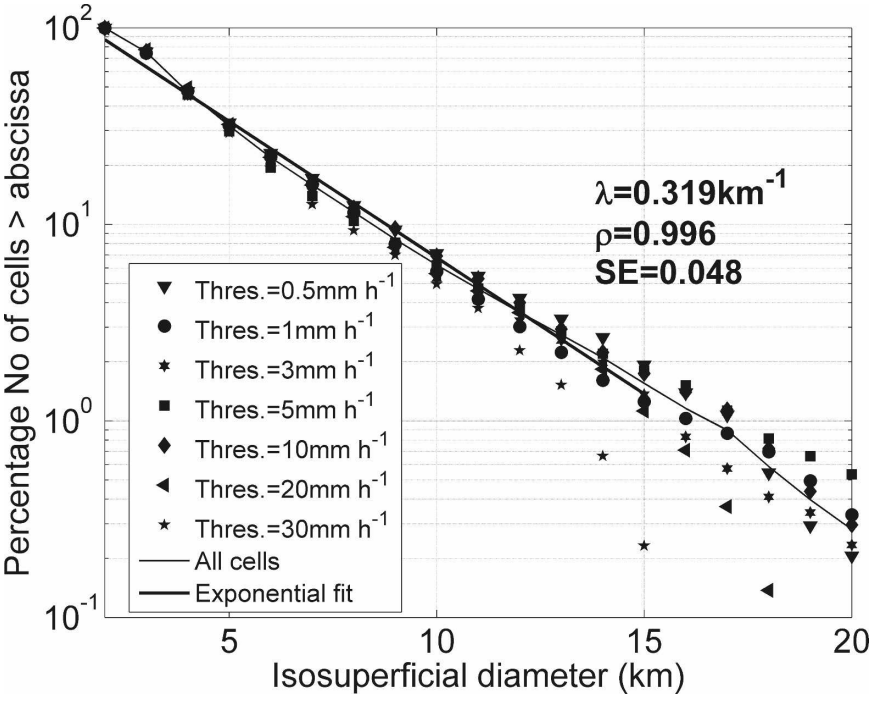

FIG. 3. Distribution of rain cell diameters, obtained from the complete database for different thresholds.

The curves show, for example, that if we choose a threshold of 3 mm h^{-1}, we have a total of about 25 000 rain cells in our complete database; if we consider only those cells that admit a valid mother, this figure reduces to about 7000 if the progenitor (i.e., the first mother of the progeny) was obtained at a threshold of 1 mm h^{-1} and to about 4000 if the progenitor was obtained from a threshold of 0.5 mm h^{-1}.

This means that, for a given partial database, the rain cells defined at different thresholds are almost uncorrelated because, at every threshold, a huge number of "orphan" structures without any parental connection to other cells is identified. The very low correlation among rain cells at different thresholds ensures the consistency of the statistical analyses presented in section 6. With respect to structures that have a mother, the orphans are characterized by greater area and perimeter, lower peak and average value of rain rate, cell dynamic close to one, and solidity values close to zero; this can be explained observing that the orphans derive from "invalid" mothers (i.e., rain cells large enough to intercept the radar observation window). They are usually associated with stratiform events characterized by great extension, flat dynamic, and high spatial complexity.

On the contrary, no significant difference in cell ellipticity (i.e., cell shape) can be observed between daughters and orphans.

When the value of the threshold is increased, rain cells become smaller; valid mothers may fragment, forming several daughters, or they may disappear. Moreover, "new" structures enter the database, derived from mothers that were invalid (too large) at the lower threshold. To quantify the degree of fragmentation and disappearance for every threshold, rain cells have been classified on the basis of the number of daughters

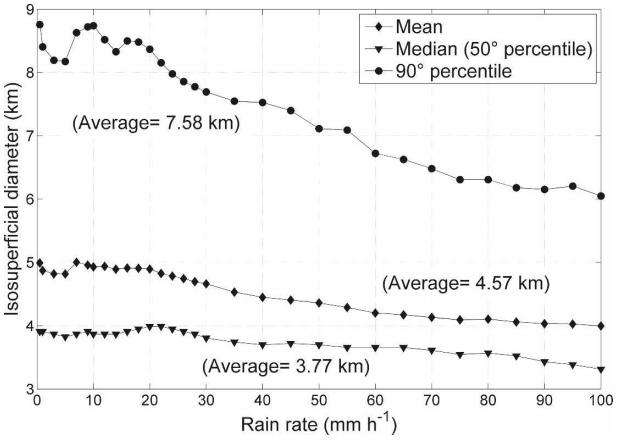

FIG. 4. Average, median, and 90% percentile isosuperficial diameter vs rain rate. The figures in parentheses represent the average values computed over the whole rain-rate range.

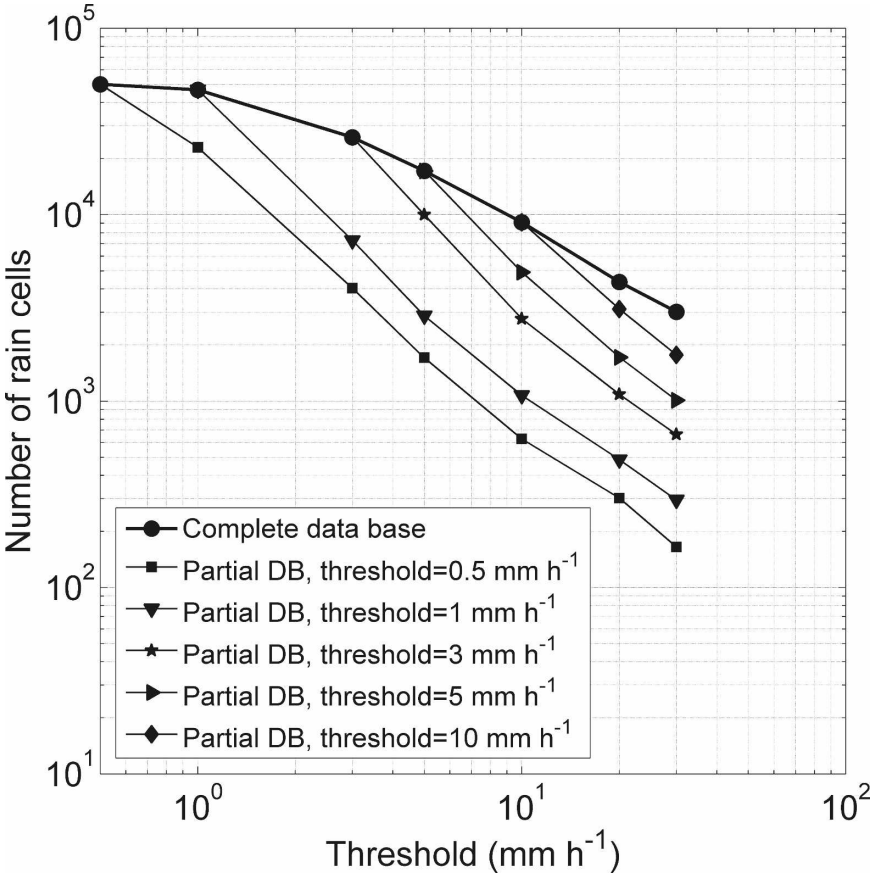

FIG. 5. Cardinality of rain cells collected in the databases for different thresholds.

produced at the following threshold. The results are presented in Fig. 6, which shows the preponderance of disappearance over fragmentation at every threshold.

The percentage of rain cells that "survive" at the successive threshold increases with the threshold, since rain structures become more representative of convective precipitation. For example, 60% of the structures defined at 3 mm h^{-1} related to the partial database with minimum threshold equal to 0.5 mm h^{-1} disappear and 38% survives, while only 2% fragments into two or more daughter cells at 5 mm h^{-1}. This behavior is coherent with the preceding analyses where it has been outlined how the complete database is constituted—at every threshold—by a nonnegligible number of orphan structures.

Finally, we have classified mother structures on the basis of the number of daughters they generate as a function of the threshold. We found a decreasing linear relation on the semilogarithmic scale for every (mother's) threshold considered. This study has been carried out only for the lowest thresholds, where the maximum number of daughter cells is at least equal to three. Figure 7 shows the results relative to a (mother's) threshold of 0.5 mm h^{-1}; the function $y = k \times 10^{mx}$ approximates fairly well the actual data distribution.

6. Descriptors analyses

The great amount of information stored in the complete database can be exploited to investigate the statistical properties of the descriptors. In section 6a we discuss single statistics, that is, the probability density function, and the centrality, dispersion, and excursion parameters for every threshold. We have also performed nonparametric tests to verify if the actual probability density functions (pdfs) can be approximated with a known statistical distribution. In section 6b we discuss joint statistics calculated for selected pairs of descriptors characterizing rain cells at a fixed threshold, looking for possible correlations between them.

a. Single statistics

As a first step we have evaluated, for each descriptor at every rain-rate threshold, the centrality parameters'

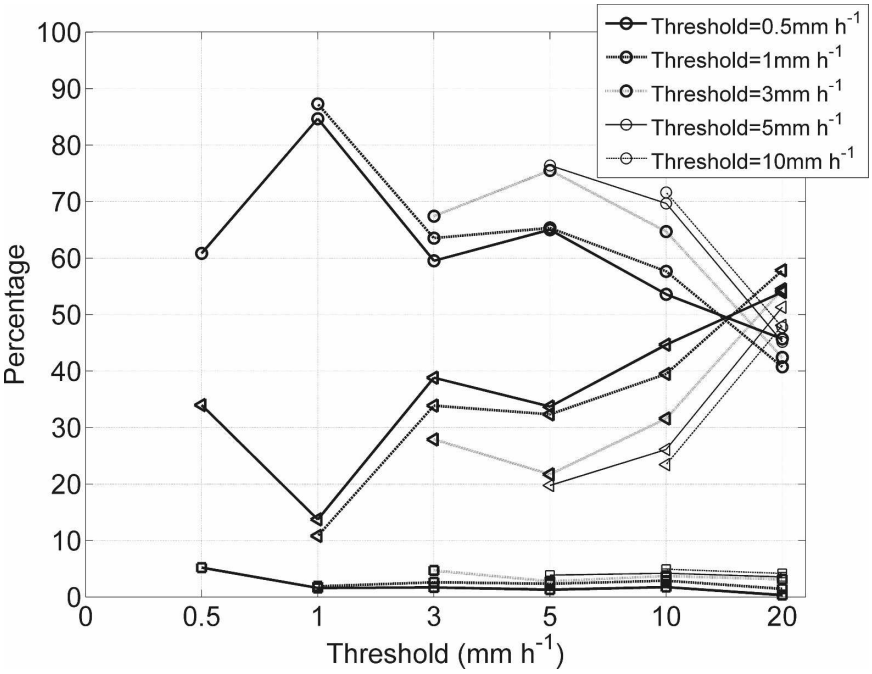

FIG. 6. Percentage of occurrence of mother cells, classified on the basis of the number of generated daughters. The lines with dots refer to rain cells without daughters (i.e., that disappear), the lines with triangles refer to cells with one daughter, and the lines with squares refer to cells with at least two daughters (i.e., that fragment). Different line types (solid, dashed, dotted, etc.) refer to different partial databases.

median and mean value, the maximum excursion through the minimum and maximum value, and the dispersion parameters standard deviation, for nonnormalized descriptors, and 90%–95% percentile for normalized ones. Figure 8 shows the results of this analysis relative to the nonnormalized descriptors: it is evident how the centrality and dispersion parameters of area and perimeter admit a negligible dependence of rain-rate level, although the maximum excursion varies with the threshold. In particular, more than 90% of the rain cells are smaller than 65 km^2 and more than 95% are smaller than 100 km^2. The maximum excursion (and, consequently, the percentiles) for diffusion, peak, and average rain rate is reduced for increasing threshold; this is due to the transition from stratiform to convective regime.

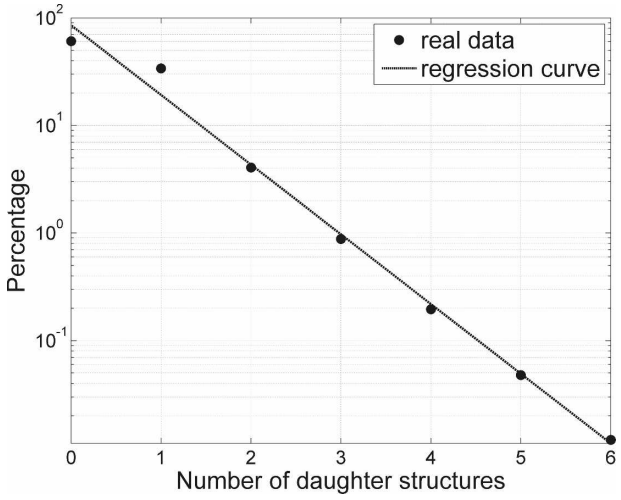

FIG. 7. Percentage of mother structures (defined at 0.5 mm h^{-1}) that generate the number of daughters on the abscissa (at the threshold of 1 mm h^{-1}). Data are related to the partial database with a minimum threshold equal to 0.5 mm h^{-1}.

Figure 9 shows the results relative to the normalized descriptors: the morphological descriptors ellipticity and solidity are almost independent of the threshold, while cell dynamic shows a behavior similar to that of peak rain rate. In particular the ellipticity admits median and mean value in the range 0.48–0.52 while the standard deviation is always lower than 0.2; this means that the rain cells tend to have an elongated shape and, on average, to be twice as long as wide. Less than 8% of the rain structures admit a "round" shape; that is, they have ellipticity greater than 0.8 (Feral et al. 2000; Pawlina 1999; Montopoli et al. 2006).

It is worthwhile to note that we found no influence of

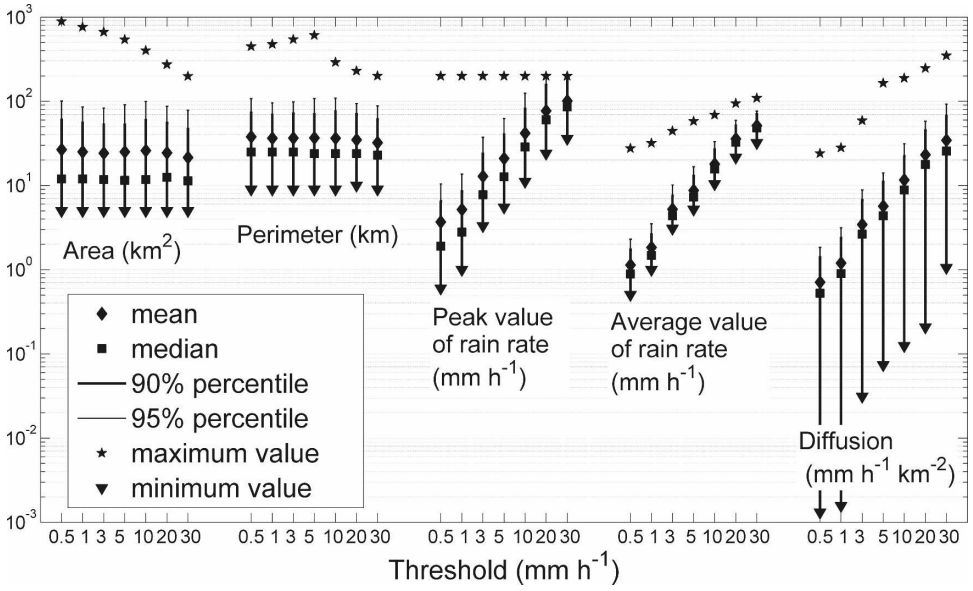

FIG. 8. Trend of the statistical parameters related to nonnormalized descriptors area, perimeter, peak, and average rain rate as a function of the threshold.

the antenna radiation diagram on the morphological descriptors: a plot of the ellipticity parameter as a function of the distance of the cell's centroid from the radar showed no correlation between the two quantities [the slope of the linear best fit (in a least squares sense) being 0.0012 and the correlation coefficient 0.053]. Moreover, the replication procedure (section 3) does not change either the statistical parameters relative to rain cells defined at thresholds greater than 10 mm h^{-1} (only very weak stratiform events are duplicated), or

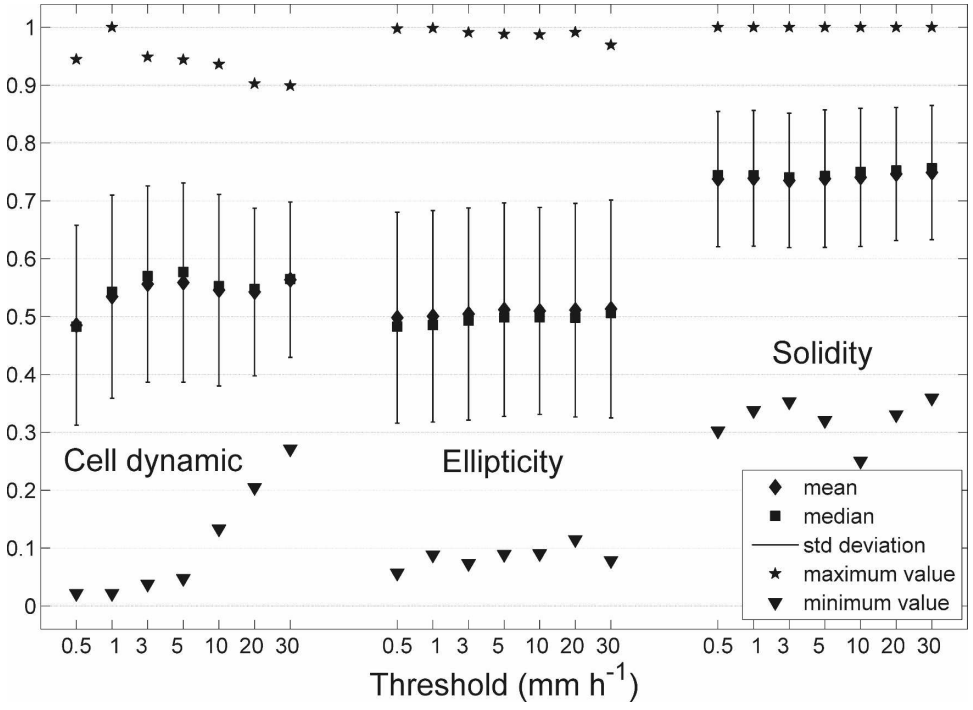

FIG. 9. Trend of the statistical parameters related to normalized descriptors dynamic, ellipticity, and solidity as a function of the threshold.

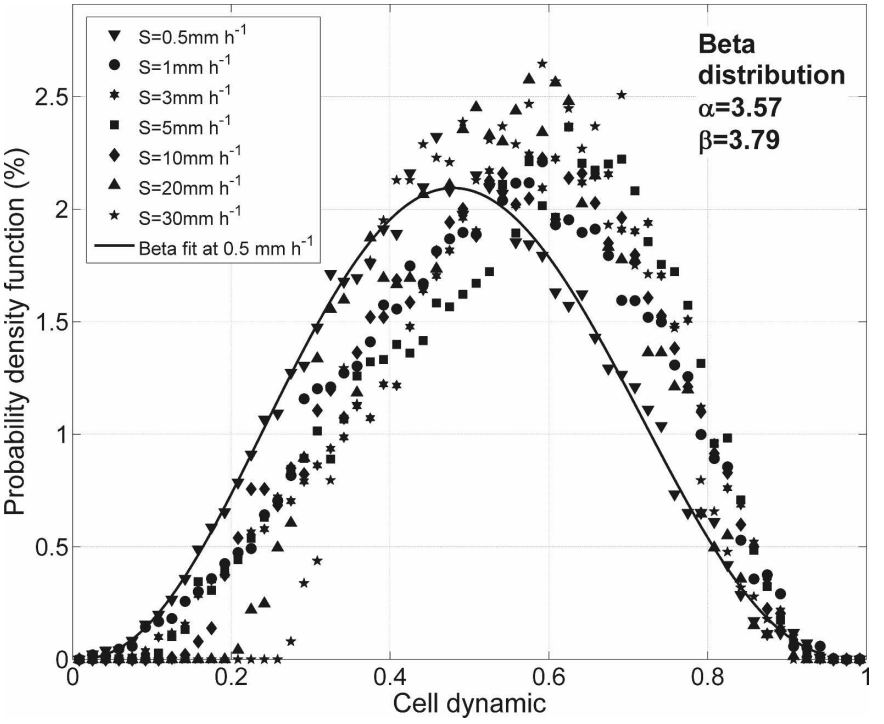

FIG. 10. Pdf of dynamic, for every threshold S; solid line shows the fit calculated for S = 0.5 m h^{-1} (beta function with parameter $\alpha = 3.57$ and $\beta = 3.79$).

the excursion of the descriptors at every threshold (the replication increases the cardinality, but it does not add new typologies of rain cells).

As a second step, we have looked for analytical functions that could approximate the actual probability density functions of the descriptors; the chi-square test (with $\alpha = 0.95$) has been adopted to verify the hypotheses, subdividing the possible range assumed by the descriptor in 20 disjoined intervals. Since the descriptors are defined in R^+, we have chosen to test the most usual statistic distributions defined in such a domain. Although the results of the tests have been negative on the whole, there are some similarities between the actual distribution functions of some descriptors and some analytical functions. In particular, dynamic distribution can be approximated with a beta distribution; Fig. 10 shows the pdfs as functions of the threshold S; the solid line is the best fit for $S = 0.5$ mm h^{-1}, a beta function with parameter $\alpha = 3.57$ and $\beta = 3.79$. Ellipticity and solidity pdfs can be modeled with a Weibull distribution, and diffusion with a lognormal function (see Fig. 11).

Area and perimeter show a decreasing exponential behavior almost independent of the rain threshold, with the curves that tend to become slightly steeper as the threshold increases. Peak and average value of rain rate admit a decreasing exponential trend whose peak value tends to increase as the rain threshold increases; this behavior is not unexpected since these descriptors are proportional to the amount of water mass present in structures, and this depends on the threshold.

b. *Joint statistics*

Looking for possible correlations, we have evaluated joint statistics for different couples of descriptors and for different thresholds; in particular, we have computed the mean values and the regression curves (using a linear, power-law, and polynomial fit). The mean values have been obtained assuming one descriptor as the independent variable (on the abscissa) and calculating the mean value of the other descriptor for a given abscissa. To investigate the nature of the correlation two "quality" parameters have been considered: the correlation coefficient ρ and the mean deviation δ. The former is defined as

$$\rho = \frac{\sigma_{xy}}{\sigma_x - \sigma_y}, \tag{3}$$

where σ_x and σ_y are the standard deviations of vectors **x** and **y**, containing, respectively, the values of independent and dependent descriptors, and σ_{xy} is their covariance. The mean deviation δ is defined through the resi-

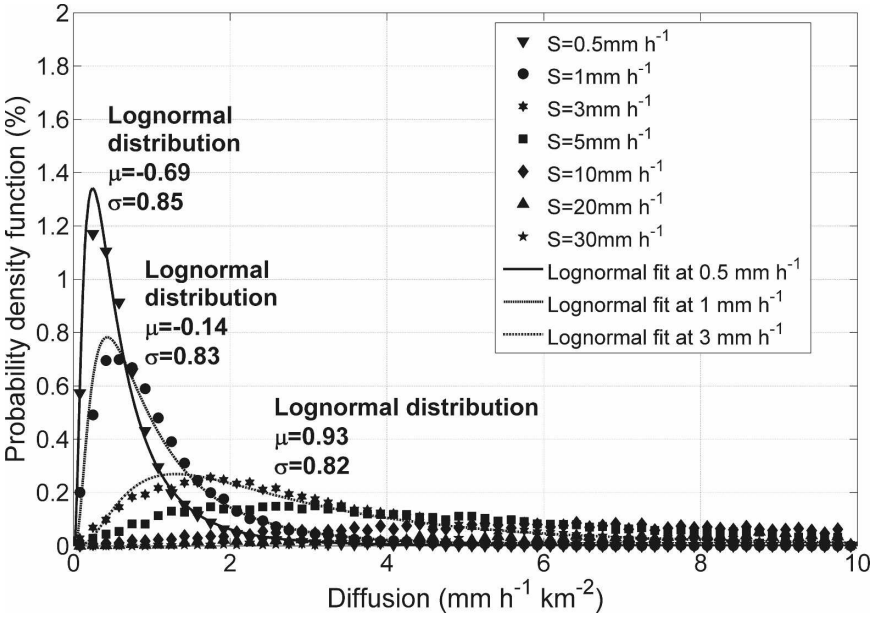

FIG. 11. Pdf of diffusion, for every threshold S; lines show the fit using a lognormal function for S = 0.5, 1, and 3 mm h^{-1}. At least 90% of rain cells with thresholds lower or equal at 5 mm h^{-1} are taken into account.

due quantity r_i, which depends on the actual value of the dependent descriptor y_i and on the value $\hat{y}_i$ assumed by the regression curve for a certain abscissa:

$$\delta = \sqrt{\frac{1}{N}\sum_{i=1}^{N} r_i^2} \quad r_i = y_i - \hat{y}_i. \tag{4}$$

In Eq. (4), N is the number of structures (i.e., couples of descriptors) considered; in case of nonlinear fitting, the only quality parameter considered is the mean deviation δ.

As a first quality check we have discarded those couples that are clearly not correlated; to this purpose, for a given value of the independent descriptor (abscissa) we have computed the interval Δ_{int}, centered around the mean value of the dependent descriptor (ordinate), which gathers 70% of samples. Only if Δ_{int} is smaller than one-third of the total width of the distribution is the regression calculated; otherwise, the distribution is assumed to be too "uniform" to show any significant correlation. These analyses have been performed for the different rain-rate thresholds to show possible dependence.

The extension of rain cells has been investigated first; comparative statistical analyses have been performed for every couple area–other descriptor and for every threshold, considering only structures with area ≤20 km^2 (that correspond to about 70% of structures stored in the database). The results of these analyses, relative to low, medium, and high rain-rate threshold, are presented in Table 2; missing figures denote the absence of the relative regression because it does not satisfy the

TABLE 2. Results of comparative statistical analyses with independent parameter area, considering structures with area smaller than or equal to 20 km^2. The unit of measure of quantity δ is the same of the dependent parameter to which δ refers.

Dependent parameter	S = 0.5 mm h^{-1}			S = 5 mm h^{-1}			S = 30 mm h^{-1}			Regression curve
	ρ	δ	Δ_{int} (%)	ρ	δ	Δ_{int} (%)	ρ	δ	Δ_{int} (%)	
Perimeter (km)	0.99	0.42	17.91	0.99	0.57	19.67	0.98	0.91	18.25	$y = ax + b$
R_{max} (mm h^{-1})	0.97	0.14	2.79	0.97	0.64	8.29			40.22	$y = ax + b$
R_{mean} (mm h^{-1})	0.97	0.03	5.98	0.96	0.16	8.10			34.43	$y = ax + b$
Dynamic		0.005	32.16		0.007	30.32		0.009	22.90	$y = cx^d$
Diffusion (mm h^{-1} km^{-2})			34.23	0.85	0.21	22.01	0.54	2.81	26.97	$y = ax + b$
Ellipticity			39.85			41.21			40.10	No
Solidity	−0.97	0.005	32.34	−0.94	0.009	32.16	−0.87	0.01	30.21	$y = ax + b$

TABLE 3. Results of comparative statistical analyses with independent parameter diffusion. The unit of measure of quantity δ is the same as the dependent parameter to which δ refers.

Dependent parameter	$S = 0.5$ mm h^{-1}			$S = 5$ mm h^{-1}			$S = 30$ mm h^{-1}			Regression curve
	ρ	δ	Δ_{int} (%)	ρ	δ	Δ_{int} (%)	ρ	δ	Δ_{int} (%)	
Area (km^2)	0.81	3.89	13.52	0.56	3.11	12.07	0.71	2.57	24.74	$y = ax + b$
Perimeter (km)	0.91	3.09	16.63	0.78	2.69	15.45	0.82	2.38	29.60	$y = ax + b$
R_{max} (mm h^{-1})	0.92	0.47	10.46	0.85	1.39	17.53			55.01	$y = ax + b$
R_{mean} (mm h^{-1})	0.91	0.07	14.25	0.80	0.27	20.13			45.26	$y = ax + b$
Dynamic			34.52			33.44	−0.54	0.02	29.19	$y = ax + b$
Ellipticity		0.006	12.74		0.007	10.67		0.009	10.30	$y = cx^d$
Solidity	−0.97	0.01	30.61	−0.96	0.01	32.47	−0.96	0.02	28.02	$y = ax + b$

hypotheses above. As can be expected, the behavior of quality parameters ρ, δ, and Δ_{int} is almost independent of the rain-rate threshold and the regression curves are a good fit for the mean curves of the three descriptors linked to the area (i.e., perimeter, dynamic, and solidity). The couple area dynamic reveals, in particular, an unexpected mutual dependence (dynamic decreases for increasing area) that is independent of the threshold.

The descriptors diffusion, peak, and average value of rain rate, which are sensitive to the threshold, have quality parameters that tend to degrade as the threshold increases because the percentage of flat structures decreases.

The high value of the Δ_{int} parameter related to the couple area ellipticity, for every threshold, tells us that there is no correlation between the size and the shape of rain cells: every area class admits rain cells of various shapes without any preferential form.

Analyses of the same kind have been performed for every couple perimeter–other descriptor, obtaining similar results, being that area and perimeter are strongly correlated. Also in this case excellent results have been obtained for the descriptors related to the perimeter (i.e., area and solidity), in terms of both quality parameters and regression curves; for the descriptors sensitive to the threshold, on the contrary, the quality parameters ρ, δ, and Δ_{int} worsen with increasing threshold. For the descriptors linked to the perimeter the regressions have been performed on 95% of the rain cells and for the thresholds not higher than 5 mm h^{-1}; for the others we have considered only structures with perimeters $\leq$35 km, which corresponds to about 70% of structures stored in the database. There is a strong correlation between the perimeter and solidity; for increasing values of the perimeter, the solidity decreases (i.e., the "roughness" increases), in particular in the interval from 10 to 20 km. Information about the complexity and roughness of rain cells can also be inferred from the relationship between area and perimeter, since a given length of "smooth" perimeter encloses more area than a "rough" one. Such a degree of spatial complexity can be quantified through the T parameter (Callaghan and Vilar 2002) in

$$P \propto \sqrt{A^T}, \tag{5}$$

where P is the perimeter and A is the area. For regular shape, $T = 1$, while as the perimeter becomes increasingly distorted, T approaches 2. The T parameter estimated for our structures, at different thresholds, has shown only a slight dependence on the threshold itself, assuming values between 1.49 and 1.54; this is an indication that the spatial characteristics of rain cells are uncorrelated with the threshold.

The analyses performed for every couple of descriptors, considering as independent parameters the peak or the average value of rain rate, led to similar results: the quality parameters ρ, δ, and Δ_{int} are strongly dependent on the rain threshold and worsen as the threshold increases, except when the dependent parameter is the dynamic; this can be expected because of its definition. Finally, the analyses executed with the morphological descriptors as dependent parameters have shown a negligible correlation.

Different behaviors have been obtained from the analyses performed assuming diffusion as an independent parameter; the results, relative to thresholds of 0.5, 5, and 30 mm h^{-1}, are presented in Table 3. It can be noted that the quality parameters ρ, δ, and Δ_{int} are strongly dependent on the rain threshold except in the case of morphological descriptors. For these cases the regression curve approximates very well the real behavior of data, independently on the threshold; Fig. 12 shows the results for the couple diffusion–ellipticity at 30 mm h^{-1}. It is clear that more elongated cells are characterized by high values of diffusion.

The statistical analyses carried out assuming dynamic, ellipticity, or solidity as independent parameters have been performed on a subset of the database, containing about 90% of the whole structures; we had to

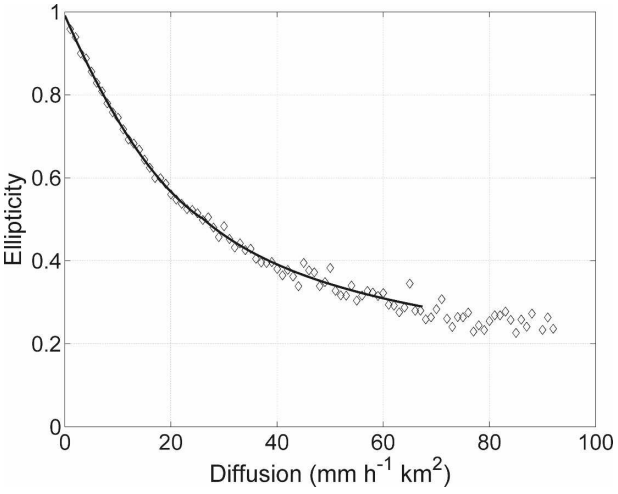

FIG. 12. Scatterplot of ellipticity vs diffusion, for a threshold of 30 mm h^{-1}. The markers represent the mean values; the solid line is the regression curve relative to 90% of the structures.

discard, in fact, outliers that are placed at the lowest values of the scale and those that are strongly dependent on the threshold. Moreover, to improve the reliability of the regression curves, the rain cells have been subdivided into two groups on the basis of their own dynamic value with respect to the peak value of the relative probability density function. In addition to the (somehow expected) excellent correlation between dynamic and peak and average rain rate, other unexpected strong correlations have been found between dynamic and both geometrical and morphological descriptors that do not degrade with the threshold. The scatterplots of area and perimeter versus dynamic show a monotone nonlinear behavior well approximated by the regression curve $y = cx^d$, while solidity shows a nonmonotone nonlinear dependence on dynamic (that can be approximated by a polynomial curve), an indication that rain cells with both a high or flat dynamic admit a more rough shape with respect to rain structures with an average dynamic.

The analyses performed for every couple of descriptors and for every threshold, considering ellipticity as the independent parameter, led to the following results: negligible correlation was found with area, perimeter, peak, and average rain rate, for every threshold; appreciable correlation was found, on the contrary, with diffusion and solidity; rain cells of elongated shape showed, for example, higher spatial complexity than rounded ones.

The analyses executed with solidity as an independent descriptor led to results different from those obtained with ellipticity; in particular our analyses revealed an appreciable degree of correlation also with area, perimeter, diffusion, peak, and average rain rate (the last three limitedly to the lowest thresholds). However, the quality parameters ρ, δ, and Δ_{int} are strongly dependent on the rain threshold, and they worsen as the threshold increases. Numerical results are presented in Table 4, where blank spaces indicate that no regression has been performed since the hypotheses about the Δ_{int} width are not satisfied.

7. Conclusions

A large database of radar maps collected in various years in the Padana Valley has been analyzed to investigate the geometrical, physical, and morphological features of rain cells, through the introduction of a set of appropriate descriptors. The cell descriptors considered are of concern for meteorological, hydrological, and telecommunication applications. For example, terrestrial and space radio communication systems operating at microwave frequencies can suffer from serious propagation impairments due to rain (i.e., attenuation, scattering interference, etc.). To predict the effectiveness of possible countermeasures (i.e., space, frequency, or time diversity), models of precipitation are needed that correctly reproduce the size and shape of the rain cells, and the rain-rate distribution inside. The statistics pre-

TABLE 4. Results of comparative statistical analyses with independent parameter solidity, considering 90% of the rain cells and excluding the outliers. The unit of measure of quantity δ is the same as the dependent parameter to which δ refers.

Dependent parameter	$S = 0.5$ mm h^{-1}			$S = 5$ mm h^{-1}			$S = 30$ mm h^{-1}			Regression curve
	ρ	δ	Δ_{int} (%)	ρ	δ	Δ_{int} (%)	ρ	δ	Δ_{int} (%)	
Area (km^2)	−0.95	3.43	12.92	−0.96	4.76	10.22	−0.87	6.67	20.67	$y = ax + b$
Perimeter (km)	−0.98	3.30	18.65	−0.96	5.66	15.75	−0.93	7.21	26.74	$y = ax + b$
R_{max} (mm h^{-1})	0.84	0.29	3.54	0.32	1.64	13.11			55.51	$y = ax + b$
R_{mean} (mm h^{-1})		0.04	2.75		0.23	16.16			37.81	$y = ax^2 + bx + c$
Dynamic			37.93			37.54		0.02	29.25	$y = cx^d$
Diffusion (mm h^{-1} km^{-2})		0.06	16.59		0.54	21.92			39.38	$y = cx^d$
Ellipticity			38.08			38.65			37.62	No

sented here are of prime importance for the development of such models.

The rain cell diameter distribution—consistent with the literature—follows an exponential form with the slope equal to 0.319 km^{-1}; the average and the median values are almost independent on the threshold. Fragmentation of rain cells is negligible with respect to disappearance, for all values of the rain intensity threshold examined (0.5–30 mm h^{-1}). Furthermore, it has been found that the number of gathered structures in relation to the number of daughter cells produced (at the next threshold) follows a decreasing exponential distribution. The analyses on the rain cell descriptors have regarded both their statistical characterization and the joint statistics between every couple of them. Single statistics have been focused on the dependence of centrality, excursion, and dispersion parameters of every descriptor on the threshold. Area, perimeter, ellipticity, and solidity show a negligible dependence on rain-rate level; on the contrary, the maximum excursion (and, consequently, the percentiles) of diffusion, dynamic, peak, and average value get narrower for increasing values of the threshold. In particular, the ellipticity admits median and mean values in the range 0.48–0.52 and a standard deviation always lower than 0.2: this means that the rain cells tend to have an elongated shape and, on average, tend to be twice as long as wide. Attention has been paid also to the probability density function of the descriptors, to verify if their trend can be approximated by a known distribution. It has been found that dynamic distribution can be approximated with a beta distribution, the ellipticity and the solidity with a Weibull, and the diffusion with a lognormal law. Through the joint analyses it has been possible to highlight important correlations between descriptors. The extension of rain cells is highly correlated with the descriptors perimeter, dynamic, and solidity, while it is uncorrelated with ellipticity. Peak and average values of rain rate are uncorrelated with morphological descriptors, a sign that in every threshold class rain cells of different shape are present. The comparative statistical analyses performed with physical descriptors as independent parameters revealed strong correlations between diffusion and the morphological descriptors and between dynamic and both geometrical and morphological descriptors. Joint statistics focused on ellipticity have revealed a strong correlation between this descriptor and both diffusion and solidity; analyses with solidity as an independent descriptor have shown correlation between this descriptor and both geometrical descriptors (area and perimeter) and physical descriptors (peak and average value of rain rate).

REFERENCES

Belongie, S., J. Malik, and J. Puzicha, 2002: Shape matching and object recognition using shape contexts. *IEEE Trans. Pattern Anal. Mach. Intel.,* **24,** 509–522.

Borga, M., E. N. Anagnostou, and E. Frank, 2000: On the use of real-time radar rainfall estimates for flood prediction in mountainous basins. *J. Geophys. Res.,* **105,** 2269–2280.

Callaghan, S. A., and E. Vilar, 2002: Spatial variation of rain fields in the south of England. *Proc. COST 280 Workshop,* Malvern, United Kingdom, European Cooperation in the Field of Scientific and Technical Research, 1–10.

Capsoni, C., and M. D'Amico, 2004: Morphological description of the rain structures in the Padana valley. *Proc. Third European Conf. on Radar Meteorology,* Visby, Sweden, ERAD, 541–544.

——, F. Fedi, C. Magistroni, A. Paraboni, and A. Pawlina, 1987a: Data and theory for a new model of the horizontal structure of raincells for propagation applications. *Radio Sci.,* **22,** 395–404.

——, ——, and A. Paraboni, 1987b: A comprehensive meteorologically oriented methodology for the prediction of wave propagation parameters in telecommunication applications beyond 10 GHz. *Radio Sci.,* **22,** 387–393.

Cheng, M. D., and A. Arakawa, 1997: Inclusion of rainwater budget and convective downdrafts in the Arakawa–Schubert cumulus parametrization. *J. Atmos. Sci.,* **54,** 1359–1378.

Davarian, F., 1994: Earth-satellite propagation research. *IEEE Commun. Mag.,* **32,** 74–78.

Dell'Acqua, F., and P. Gamba, 1998: Modal morphing on meteorological radar data for rainfall pattern analysis. *IEE Proc. Radar Sonar Navig.,* **145,** 123–127.

——, ——, and A. Marazzi, 1997: Tracking the evolution of rain patterns by means of modal matching. *IEEE Trans. Geosci. Remote Sens.,* **4,** 1463–1465.

Drufuca, G., and A. Pawlina, 1976: Some statistics of radar precipitation patterns. Preprints, *17th Conf. on Radar Meteorology,* Seattle, WA, Amer. Meteor. Soc., 438–441.

Feral, L., F. Mesnard, H. Sauvageot, L. Castanet, and J. Lemorton, 2000: Rain cells shape and orientation distribution in south-west of France. *Phys. Chem. Earth,* **25B,** 1073–1078.

Franchi, G., P. Gamba, A. Marazzi, and A. Mecocci, 1996: Object tracking in complex scenes by means of the correspondence based method. *Proc. Eighth Mediterranean Electrotechnical Conf.,* Ajaccio, France, Institute of Electrical and Electronics Engineers, 1093–1096.

Fukuchi, H., P. A. Watson, and A. F. Ismail, 2000: Proposal of novel attenuation mitigation technologies for future millimetre-wave satellite communications. *Proc. AP2000 Millennium Conf. on Antennas and Propagation,* Davos, Switzerland, European Space Agency, 1–4.

Georgakakos, K. P., and W. F. Krajewski, 1996: Statistical-microphysical causes of rainfall variability in the tropics. *J. Geophys. Res.,* **101** (D21), 26 165–26 180.

Goldhirsh, J., 1982: Space diversity performance prediction for earth satellite paths using radar modelling techniques. *Radio Sci.,* **17,** 1400–1410.

——, 1983: Rain cell size statistics as a function of rain rate for attenuation modelling. *IEEE Trans. Antennas Propag.,* **31,** 799–801.

——, and B. H. Musiani, 1986: Rain cell size statistics derived from radar observations at Wallops Island, Virginia. *IEEE Trans. Geosci. Remote Sens.,* **24,** 947–954.

——, and ——, 1992: Dimension statistics of rain cell cores and associated rain rate isopleths derived from radar measurements in the mid-Atlantic coast of the United States. *IEEE Trans. Geosci. Remote Sens.,* **30,** 28–37.

Khamis, N. H. H., J. Din, and T. A. Rahman, 2005: Analysis of rain cell size distribution from meteorological radar data for rain attenuation studies. *Proc. Asian-Pacific Conf. on Applied Electromagnetics,* Johor, Malaysia, Institute of Electrical and Electronics Engineers, 118–120.

Konrad, T. G., 1978: Statistical models of summer rainshowers derived from fine-scale radar observations. *J. Appl. Meteor.,* **17,** 171–188.

Li, L., W. Schmid, and J. Joss, 1995: Nowcasting of motion and growth of precipitation with radar over a complex orography. *J. Appl. Meteor.,* **34,** 1286–1300.

Matricciani, E., and A. Pawlina, 2000: Statistical characterization of rainfall structure and occurrence for convective and stratiform rain inferred from long term point rain rate data. *Proc. AP2000 Millenium Conf. on Antennas and Propagation,* Davos, Switzerland, European Space Agency, 1–4.

Mecklenburg, S., V. A. Bell, R. J. Moore, and J. Joss, 2000: Interfacing an enhanced radar echo tracking algorithm with a rainfall-runoff model for real time flood forecasting. *Phys. Chem. Earth,* **25B,** 1329–1333.

Montopoli, M., F. S. Marzano, G. Vulpiani, A. Fornasiero, P. P. Alberoni, L. Ferrarsi, and N. Rebora, 2006: Spatial characterization of raincell horizontal profiles from C-band radar measurements at mid-latitude. *Adv. Geosci.,* **7,** 285–292.

Oguchi, T., 1983: Electromagnetic wave propagation and scattering in rain and other hydrometeors. *Proc. IEEE,* **71,** 1029–1078.

Paraboni, A., C. Capsoni, G. Masini, J. P. V. Poiares Baptista, and C. Riva, 2002: Dynamic fade restoration in Ka-band satellite systems. *Int. J. Satell. Commun.,* **20,** 283–292.

Pawlina, A., 1984: Some features of ground rain patterns measured by radar in north Italy. *Radio Sci.,* **19,** 855–861.

——, 1987: Radar rain patterns: Automatic extraction, collection and description for modeling purposes. *Alta Freq.,* **LVI,** 153–159.

——, 1990: Friendly access to radar images: Advanced database hosting rain maps, patterns, their descriptors and models. *Proc. Int. Telecommunication Symp.,* Rio de Janeiro, Brazil, Institute of Electrical and Electronics Engineers, 72–76.

——, 1998: Current knowledge of horizontal rain structures for Sat-Com oriented models. *Proc. ESA First Int. Workshop on Radio Wave Propagation Modelling for SatCom Services at Ku-band and Above,* Noordwijk, Netherlands, European Space Research and Technology Center, 161–174.

——, 1999: Essential knowledge of rain structure for radio applications based on available data and models. *Proc. Third Regional Workshop on Radio Communication in Africa,* Gaborone, Botswana, University of Botswana, 1–11.

Sauvageout, H., F. Mesnard, and R. S. Tenorio, 1999: The relation between the area-average rain rate and the rain cell size distribution parameters. *J. Atmos. Sci.,* **56,** 57–70.